

# High-pressure $^{155}\text{Gd}$ Mössbauer experiments on Gd intermetallic compounds compared with first-principles band-structure calculations

F. M. Mulder

*Kamerlingh-Onnes Laboratory, Leiden University, P.O. Box 9506, 2300 RA Leiden, The Netherlands  
and Interfaculty Reactor Institute, Delft University of Technology, Mekelweg 15, 2629 JB Delft, The Netherlands*

R. Coehoorn

*Philips Research Laboratories, Prof. Holstlaan 4, 5656 AA Eindhoven, The Netherlands*

R. C. Thiel and K. H. J. Buschow

*Kamerlingh-Onnes Laboratory, Leiden University, P.O. Box 9506, 2300 RA Leiden, The Netherlands*

(Received 16 July 1996)

High-pressure  $^{155}\text{Gd}$  Mössbauer measurements on Gd metal,  $\text{GdCo}_5$ ,  $\text{GdRu}_2\text{Si}_2$ , and  $\text{Gd}_2\text{Co}_{17}\text{N}_3$  were performed at 4.2 K. The maximum pressures reached were about 18 GPa. The resulting volume reductions of 20–30 % were determined using high-pressure x-ray diffraction. The pressure dependence of the electric-field gradients and hyperfine fields obtained for the first three systems was compared with predictions from first-principles band-structure calculations. Significant changes of the hyperfine parameters are observed, especially for elemental Gd metal. With increasing pressure, an increase of the electron density at the Gd nuclei is found in all compounds. The values of the hyperfine field initially increase with pressure. For Gd metal the induced structural phase transitions result in large changes in the electric-field gradient at the nucleus ( $V_{zz}$ ). The intermetallic compounds show no structural phase transitions and relatively small changes in  $V_{zz}$ . The combination of experiment and calculations indicates that the transition-metal magnetic moments decrease at high pressure. Although for zero pressure predictions of the electric-field gradient and the hyperfine fields, based on the calculations, are quite accurate, the calculated pressure dependence of the hyperfine parameters for Gd,  $\text{GdCo}_5$ , and  $\text{GdRu}_2\text{Si}_2$  does not in all cases lead to a satisfactory agreement with experiment. The application of pressures therefore may give additional stimulus for the improvement of the theoretical description of band structures and hyperfine parameters. [S0163-1829(97)00133-1]

## I. INTRODUCTION

In the past century the strength of permanent magnets has followed an exponential growth with time, and new developments continue.<sup>1</sup> During the last decades improvements have been made in permanent magnet materials consisting of rare-earth intermetallic compounds. The high magnetic anisotropy required is provided by the rare-earth sublattice, while a high magnetic ordering temperature and magnetization stems from transition elements like iron or cobalt. The permanent magnet materials with the best intrinsic properties often contain a third element like boron, nitrogen, or carbon.

The intrinsic properties of a rare-earth intermetallic compound determine the maximum strength that it can reach when applied as permanent magnet. Other factors, like the microstructure that can be realized during the production process, and the incorporation of secondary phases, are equally important for the performance of the permanent magnet.

In a crystal, the valence electrons of the rare-earth atom hybridize (except for the  $4f$  electrons) with those of the nearest neighbor atoms. The charge cloud of the  $4f$  shell is usually located relatively close to the nucleus, which prevents it from participating in the chemical bonding between the atoms. Depending on the crystal structure and on the other elements in the compound, a nonspherical potential results at the site of the  $4f$  electrons (the ‘‘crystal field’’).

The principal crystal field parameter is  $A_2^0$ . Depending on the rare-earth element, the charge cloud of the  $4f$  shell (in the presence of the exchange field resulting from the neighboring magnetic atoms) can have a more disc-like (‘‘oblate’’), or a more rugby-ball-like (‘‘prolate’’) shape. The electrostatic interaction of this nonspherical charge cloud with the crystal field causes the  $4f$  charge cloud, and its magnetic moment, to be oriented in a preferential crystallographic direction. This is the main factor determining the magneto-crystalline anisotropy of the rare-earth sublattice.<sup>2,3</sup>

As part of a systematic study on the origin of the crystal field, several series of compounds have been studied.<sup>2,4,5</sup> Employing  $^{155}\text{Gd}$  Mössbauer spectroscopy (MS), the electric-field gradient (EFG) at the *nuclear site* can be measured. The principal component of the EFG is  $V_{zz}$  ( $=\partial^2 V/\partial z^2$ ), in which the  $z$  direction is parallel to the  $c$  axis of the tetragonal, rhombohedral, or trigonal system studied). Gadolinium MS is especially useful, since Gd has a half-filled, spherical  $4f$  shell which thus gives no contribution to the EFG at the nucleus. The EFG has therefore the same origin as the crystal field experienced by the  $4f$  electron cloud. Since the  $4f$  shell takes virtually no part in the chemical bonds between the elements, the crystal field parameter found for a Gd compound can also be used for isomorphous compounds of other trivalent rare earths.

Coehoorn *et al.*<sup>2</sup> showed that the main factor causing the

EFG at the Gd nucleus is the asphericity of the  $6p$  and  $5d$  valence electron densities of Gd itself. This on-site asphericity is caused by the hybridization with the neighboring element valence electron states. In these studies,  $^{155}\text{Gd}$  Mössbauer results and band-structure calculations were compared. The implication is that the EFG is quite a *local* property, and less a property of the whole lattice. It was found that a phenomenological relationship of the type  $A_2^0 = -\omega V_{zz}$  exists, although it was also shown that a concise physical basis for this relation is absent.

Zero-pressure band-structure calculations are generally quite successful in describing the observed *trends* in the values of EFG and the magnetic hyperfine field ( $B_{\text{hf}}$ ) as a function of the constituting elements. The numerical values can show systematic deviations, however. In order to get an even better understanding of the behavior of the EFG and  $B_{\text{hf}}$ , and to test the accuracy of the calculations, it appeared desirable to vary a key parameter of the calculations, namely the unit cell volume. Experimentally, this can be done by applying a large hydrostatic pressure, and measuring the  $^{155}\text{Gd}$  Mössbauer spectra and the lattice parameters as a function of the pressure.

The high-pressure experiments were performed for Gd metal,  $\text{GdCo}_5$ ,  $\text{GdRu}_2\text{Si}_2$ , and  $\text{Gd}_2\text{Co}_{17}\text{N}_x$ . Gd metal is relatively soft, and therefore large effects may be expected.  $\text{GdCo}_5$  has the hexagonal  $\text{CaCu}_5$  structure and it is related to the strong permanent magnet  $\text{SmCo}_5$ .  $\text{GdRu}_2\text{Si}_2$  has the tetrahedral  $\text{ThCr}_2\text{Si}_2$  structure. It has a very large EFG at zero pressure.  $\text{Gd}_2\text{Co}_{17}\text{N}_x$  is one of the newly found  $\text{Th}_2\text{Zn}_{17}$ -type compounds with the elements N or C at an interstitial lattice position. In these compounds, Co carries a magnetic moment while Ru does not. The measurements are the first high-pressure  $^{155}\text{Gd}$  MS measurements on Gd compounds published in literature. The experimental results on Gd metal have been previously published by us.<sup>6</sup>

## II. EXPERIMENTAL PROCEDURES AND HIGH-PRESSURE APPARATUS

For the MS measurements we used a diamond anvil cell (DAC) as described in Refs. 7 and 8. The diamonds are of 0.29 carats, and have 0.8 mm diameter flat tips. In Fig. 1 a cross sectional view of the DAC is presented. Due to the high  $\gamma$ -ray energy  $E_\gamma$ , the Mössbauer Debye-Waller factors are small, and cooling of source and DAC with absorber is necessary. The entire DAC is also relatively transparent for the high energy gammas, which calls for special measures to ensure adequate shielding. The typical (powdered) sample used in experiments up to 20 GPa (=200 kbar) is 70  $\mu\text{m}$  thick and 0.4 mm in diameter, before pressurizing. The gasket material consisted of 200  $\mu\text{m}$  thick tungsten or  $\text{Pt}_{80}\text{Ir}_{20}$  sheet, preindented to a thickness of about 100  $\mu\text{m}$ .

Pressure was applied stepwise at room temperature. A pressure transmitting medium was used for obtaining a fairly hydrostatic pressure. Pressure calibration was performed *in situ* and at low temperature with the ruby fluorescence method.<sup>9,10</sup> Fine ruby chips were included in the sample chamber. The ruby fluorescence was excited by a 5 mW green HeNe laser (543.5 nm). The pressure calibration error amounted to not more than 0.3 GPa which made it possible

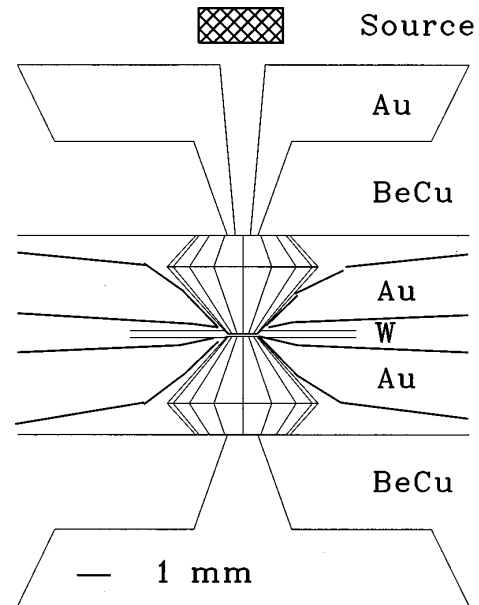


FIG. 1. A cross sectional view of the diamond anvil cell used for the MS experiments, with the Au-Pt alloy shielding.

to occasionally observe pressure inhomogeneities of a few percent.

The Mössbauer source consisted of  $\text{SmPd}_3$ , enriched to 96% in  $^{154}\text{Sm}$  which was prepared as described in Ref. 8 in order to get as high an activity as possible. The countrate obtained was about  $5 \times 10^3 \text{ s}^{-1}$   $\gamma$ -ray photons (slightly depending on the sample) of the Mössbauer transition at 86 keV. Nevertheless, due to the small resonant absorption, typical measurement times were 2 weeks per spectrum. All spectra have been analyzed by means of a least-squares fitting procedure, involving diagonalization of the full nuclear Hamiltonian and using a transmission integral. The independently refined variables consisted of the isomer shift (IS), the effective hyperfine field ( $B_{\text{hf}}$ ), and the quadrupole splitting (QS). From the last quantity, the EFG tensor element  $V_{zz}$  was obtained. The angle  $\theta$  between the hyperfine field and the  $c$  axis was kept as an adjustable parameter. The source linewidth at 4.2 K was calibrated to be  $0.37 \text{ mm s}^{-1}$ , which equals the normal value,<sup>15</sup> the absorber linewidth equals the natural linewidth of  $0.25 \text{ mm s}^{-1}$ .

High-pressure x-ray diffraction on Gd metal has been performed by Akella *et al.*,<sup>11</sup> and also by other authors.<sup>12,13</sup> They were also able to determine the structural changes that Gd exhibits. A general difficulty with high-pressure x-ray diffraction is that the diamond anvil cell limits the maximum scattering angle as well as the x-ray intensities. In several high-pressure x-ray diffraction experimental setups existing, the energy dispersive method is used. The x-rays are often produced by tunable high intensity synchrotron sources.<sup>14</sup> We studied the other compounds at high pressure with a special design diamond anvil cell, using a conventional x-ray source with a Mo target. Powder x-ray diffraction patterns were recorded in transmission scattering geometry at several pressures. Since we perform a powder diffraction experiment, the small amount of powder has to be sufficiently finegrained (grain size  $\leq 40 \mu\text{m}$ ), in order to get a good directional averaging and clear diffraction rings. The tungsten carbide backing plates of the diamonds have a conical

aperture with an opening angle of  $30^\circ$ . This limits the maximum  $2\theta$  angle realizable to  $30^\circ$ . As gasket material, the same tungsten foil as employed in the Mössbauer measurements was used. Above about 8 GPa a diffraction line of tungsten becomes visible (due to the decreased thickness of the gasket). Strong broad dots of the single-crystal diamonds are always present. The special DAC and the x-ray apparatus was kindly provided to us by Wijngaarden and de Groot from the Free University in Amsterdam.

The detection of the low intensity x-ray beam was only possible with a commercial ‘‘image plate.’’ The intensity is low because of the small sample size and the attenuation by the diamonds and the sample. The image plate absorbs the x rays efficiently (up to 90%). The high sensitivity and the possibility of image processing are big advantages over normal Röntgen films. The recording of one x-ray photograph takes about 40 min. The image plates used were kindly provided by the Onze Lieve Vrouwe Gasthuis (OLVG) hospital in Amsterdam.

### III. EXPERIMENTAL RESULTS

In general, the signal-to-noise ratios of the high-pressure spectra are not high because of the low absorption intensity and the low counting rates. Fortunately the intermetallic compounds have relatively simple spectra: they show a doublet, the distance between the two peaks roughly being determined by  $V_{zz}$ , the width by  $B_{\text{hf}}$ , and the center of mass by the IS. The spectra and fits are shown in Fig. 2, the results are displayed in Tables I and II. Although the signal to noise ratio is not high, the IS value is accurate to  $\pm 0.01$  mm/s. Typical errors for the high-pressure data are  $\pm 0.3 \times 10^{21}$  V m $^{-2}$  for  $V_{zz}$ , and  $\pm 1$  T for  $B_{\text{hf}}$ . For Gd metal a few assumptions were necessary to analyze the spectra, as was already described in Ref. 6. With increasing pressure the structure of Gd transforms from hexagonal towards a more and more cubic structure: from hcp to a Sm-type structure at 1.5 GPa, and from Sm type to dhcp at 6.5 GPa. The main assumption is that  $V_{zz}$  is restrained to zero for the site with cubic *local* symmetry.

The results of the high-pressure x-ray diffraction are plotted in Fig. 3. The intermetallic compounds show no crystallographic phase transitions or distortions at the pressures reached. This is consistent with the Mössbauer results.

### IV. FIRST-PRINCIPLES BAND-STRUCTURE CALCULATIONS

The first-principles band-structure calculational method used is described in detail in Refs. 2 and 3 and references cited therein.  $V_{zz}$  and  $B_{\text{hf}}$  are calculated and  $A_2^0$  can also be calculated within the model. We have not attempted to calculate to isomer shift. The augmented spherical wave (ASW) method employing the atomic sphere approximation (ASA) is used. Exchange and correlation effects are taken into account by the local spin density approximation (LSDA). It was shown that the main contribution to  $V_{zz}$  is that of the  $6p$  and  $5d$  valence electrons of Gd itself. Their total contribution is called  $V_{zz}(\text{val})$ .

The electronic charge densities are expressed in terms of the spin-polarized occupation numbers of Gd  $6p$  and  $5d$

valence electron states.  $V_{zz}(\text{val}) = \sum_{p,d} \sum_{\sigma} V_{zz}^{p,d,\sigma}(\text{val})$  follows from equations

$$V_{zz}^{p,\sigma}(\text{val}) = \frac{4}{5} \frac{|e|}{4\pi\epsilon_0} \left\langle \frac{S(r)}{r^3} \right\rangle_{p,\sigma} \Delta n_{p,\sigma},$$

$$V_{zz}^{d,\sigma}(\text{val}) = \frac{4}{7} \frac{|e|}{4\pi\epsilon_0} \left\langle \frac{S(r)}{r^3} \right\rangle_{d,\sigma} \Delta n_{d,\sigma}. \quad (1)$$

The constants  $\frac{4}{5}(|e|/4\pi\epsilon_0)$  and  $\frac{4}{7}(|e|/4\pi\epsilon_0)$  may be replaced by 7.74 and 5.54, respectively, when  $V_{zz}(\text{val})$  is expressed in units of  $10^{21}$  V m $^{-2}$  and  $\langle S(r)/r^3 \rangle$  in  $a_0^{-3}$  ( $a_0$  is the Bohr radius = 0.5292 Å). The quantities  $\Delta n_{p,\sigma}$  and  $\Delta n_{d,\sigma}$  represent the asphericities of the  $6p$  and  $5d$  shells with spin  $\sigma$ , and are given by the equations

$$\Delta n_{p,\sigma} = \frac{1}{2}(n_{x,\sigma} + n_{y,\sigma}) - n_{z,\sigma},$$

$$\Delta n_{d,\sigma} = n_{x^2-y^2,\sigma} + n_{xy,\sigma} - \frac{1}{2}(n_{xz,\sigma} + n_{yz,\sigma}) - n_{z^2,\sigma}, \quad (2)$$

where  $n_{x,\sigma}$ ,  $n_{y,\sigma}$ , and  $n_{z,\sigma}$  are occupation numbers of the Gd  $6p$  orbitals, and  $n_{x^2-y^2,\sigma}$ ,  $n_{xy,\sigma}$ ,  $n_{xz,\sigma}$ ,  $n_{yz,\sigma}$ , and  $n_{z^2,\sigma}$  are occupation numbers of the Gd  $5d$  orbitals. The quantities  $\langle S(r)/r^3 \rangle_{p,\sigma}$  and  $\langle r^{-3} \rangle_{d,\sigma}$  are the expectation values of the radial parts of the  $6p$  and  $5d$  wave functions weighed with  $r^{-3}$ . The function  $S(r)$  arises in a relativistic treatment of the EFG, and has been given in Ref. 16.

The magnetic hyperfine field measured at the nucleus is caused by the Fermi-contact, orbital, and dipolar interactions. For Gd, the latter two can be neglected, since they give contributions of 1 T or less. The Fermi-contact hyperfine field stems from the electron spin density near the nucleus, with the predominant contribution from the region within the Thomson radius  $r_T$ .<sup>16</sup> For Gd,  $r_T = 180$  fm, much larger than the nuclear radius which equals about 6 fm.<sup>2</sup> Results of first-principles calculations of hyperfine fields on Gd nuclei in a large number of intermetallic compounds at zero pressure have been reported by Coehoorn and Buschow.<sup>2,17</sup> It was found that calculated hyperfine fields are in very good agreement with experiment, provided a correction is made for a systematic error of about 35 T. Systematic errors have also been found in calculations of the hyperfine field of Fe, Co, and Ni,<sup>18</sup> and have been ascribed to a failure of the LSDA to accurately treat the exchange interaction between the spin-polarized  $3d$  shell, and the  $s$ -type core electrons.<sup>16,19</sup> It is an open question whether for the case of Gd a similar explanation may be given. In view of this unresolved and possibly quite fundamental issue, the comparison between theory and experiment of the pressure dependence of hyperfine fields is of great interest.

The calculations for systems under pressure were performed using the lattice parameters and atomic positions that follow from an isotropic scaling of the unit cell using the experimental crystallographic data. For hcp Gd, GdCo<sub>5</sub>, and GdRu<sub>2</sub>Si<sub>2</sub> zero-pressure data were used; for dhcp Gd, data for  $p = 7.5$  GPa were used.<sup>20</sup> A calculation for fcc Gd was performed for the purpose of comparison. The cubic lattice parameter was chosen such that the atomic volume be equal

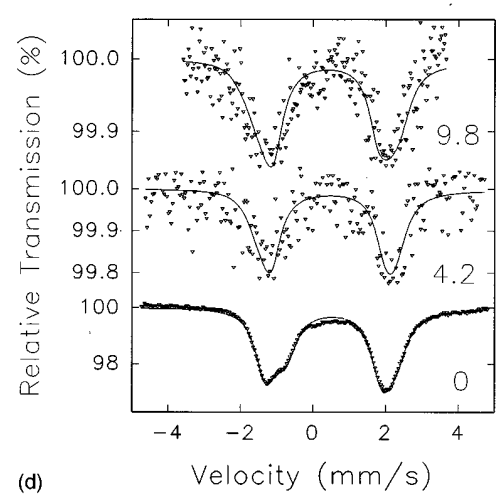
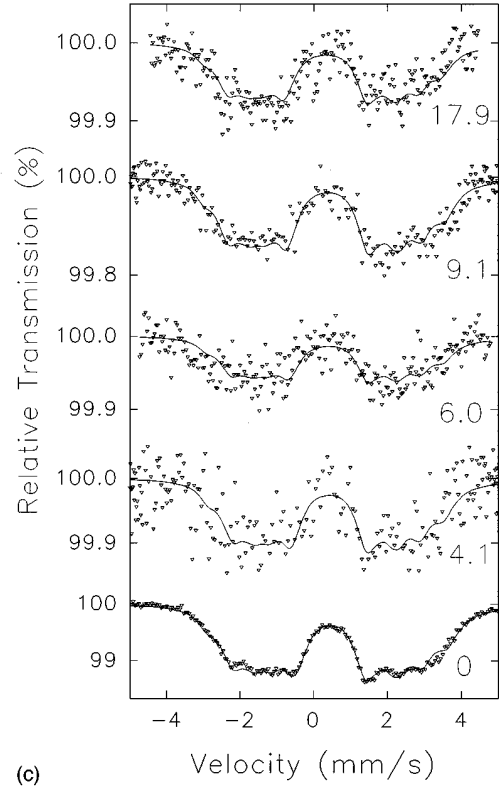
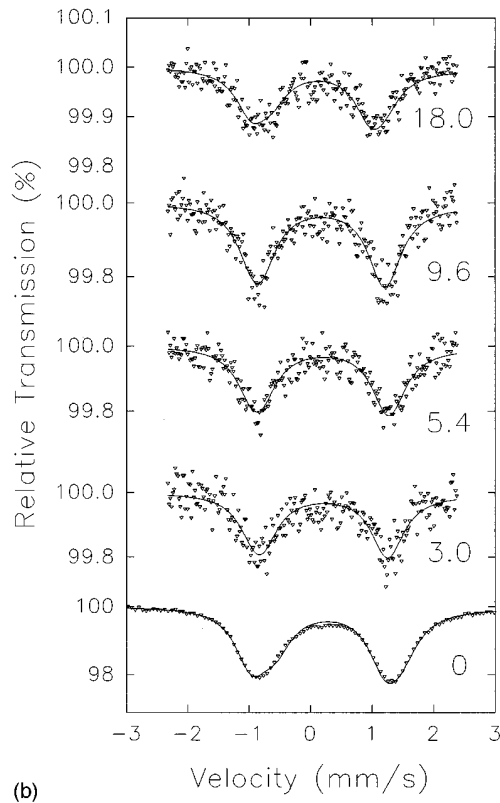
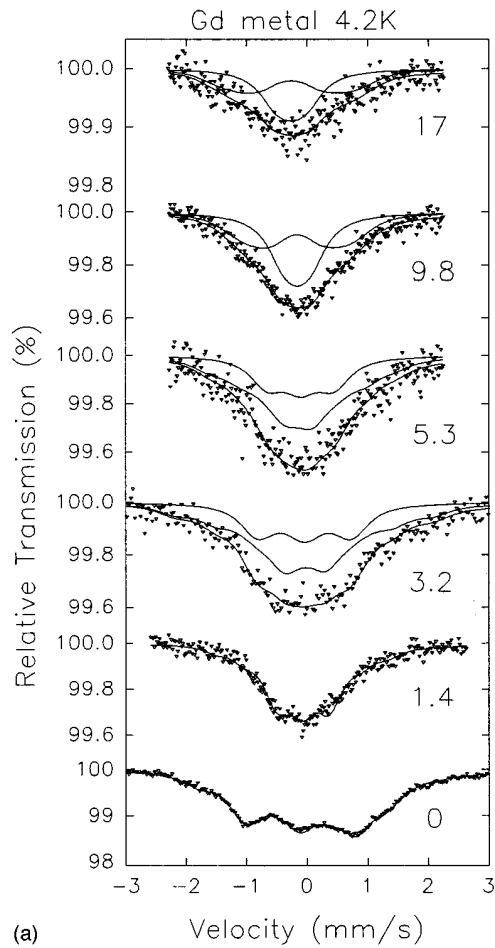


FIG. 2. Mössbauer measurements on Gd (a),  $\text{GdCo}_5$  (b),  $\text{GdRu}_2\text{Si}_2$  (c), and  $\text{Gd}_2\text{Co}_{17}\text{N}_3$  (d) at the pressures indicated in GPa, and at 4.2 K.

TABLE I. High-pressure  $^{155}\text{Gd}$  Mössbauer results for Gd metal at 4.2 K (Ref. 6). The last column gives the relative occupancies of crystallographic sites with local cubic ( $c$ ) and local hexagonal ( $h$ ) symmetry. The  $V_{zz}^{\text{hex}}$  refers to the hexagonal sites; for the cubic sites  $V_{zz}^{\text{cub}}$  was assumed to be equal to zero. For the cubic and hexagonal sites  $B_{\text{hf}}$ , IS, and  $\theta$  were assumed identical.

Pressure GPa	$V/V_0$	$V_{zz}^{\text{hex}}$ $10^{21} \text{ V m}^{-2}$	$B_{\text{hf}}$ T	IS $\text{mm s}^{-1}$	$\theta$ deg	$h:c$
0	1.00	+3.8	-39.7	+0.018	32	1:0
1.4	0.95	+4.8	-28.0	-0.08	60	1:0
3.2	0.89	+7.3	-32.5	-0.04	57	$1:\frac{1}{2}$
5.3	0.85	+5.3	-21.6	-0.11	51	$1:\frac{1}{2}$
9.8	0.78	+6.6	-9.5	-0.16	52	1:1
17.0	0.70	+8.0	+10.7	-0.25	52	1:1

to that for hcp Gd at  $p=0$ . Calculations at  $p=0$  have been performed using the following data:

Gd(hcp):  $a=3.636 \text{ \AA}$ ,  $c/a=1.590$  47,

Gd(fcc):  $a=5.097 \text{ \AA}$ ,

Gd(dhcp):  $a=3.636 \text{ \AA}$ ,  $c/a=3.247$  21.

GdCo<sub>5</sub>:  $a=4.973 \text{ \AA}$ ,  $c/a=0.798$  11,

GdRu<sub>2</sub>Si<sub>2</sub>:  $a=4.1588 \text{ \AA}$ ,  $c/a=2.3072$ ;  $z=0.38$ .

We have not performed calculations for Gd<sub>2</sub>Co<sub>17</sub>N<sub>3</sub> under pressure. The atomic sphere radii were varied in proportion to the unit cell volume. For GdCo<sub>5</sub> we used  $r_{\text{Gd}}:r_{\text{Co}}=1.35:1$  and for GdRu<sub>2</sub>Si<sub>2</sub> we used  $r_{\text{Gd}}:r_{\text{Ru}}:r_{\text{Si}}=1.23:1:1$ .

The results of the calculations are given in Table III (total and partial magnetic moments at Gd sites) and in Tables V–VIII (EFG's and hyperfine fields). The calculations for GdCo<sub>5</sub> revealed a discontinuity in the variation of the magnetic moments with the volume. This becomes apparent from Fig. 4, which shows the volume dependence of the magnetic moments at the two Co sites. A stable high moment state is found at and above a reduced volume  $V/V_0=0.90$ . At  $V/V_0=0.90$  we find a second, metastable, solution with a total energy per unit cell which is only 3 meV higher than

that for the stable, high moment solution. In the figure, the corresponding magnetic moments are indicated with an open circle. In the tables, the data for  $V/V_0=0.90$  correspond to the stable high moment state. For  $V/V_0=0.87$  and  $0.84$  we find only one stable solution. In GdRu<sub>2</sub>Si<sub>2</sub> there is a very small induced moment at the Ru sites, equal to  $-0.05$ ,  $-0.04$ , and  $-0.03\mu_B$  for reduced volumes equal to 1.00, 0.91, and 0.83, respectively (Table VIII). Moments at Si are within  $\pm 0.005\mu_B$  equal to zero at all volumes considered.

In the calculations presented above the effect of a possible change of the  $c/a$  ratios with pressure has been neglected. We have investigated this issue by performing a number of additional calculations for hcp Gd and GdCo<sub>5</sub>. The results are given in Table IV. For hcp Gd, we have varied  $c/a$ , while keeping the volume per atom equal to the experimental volume. As far as we know, the experimental information available does not show a pressure dependence of the  $c/a$  ratio for hcp Gd. In Ref. 11 no change in  $c/a$  is reported. For GdCo<sub>5</sub> x-ray diffraction shows that the  $c/a$  ratio decreases from 0.798 for  $V/V_0=1$  to 0.764 for  $V_0=0.9$ . In Table IV results of calculations for both  $c/a$  ratios, using the same unit cell volume, are given for  $V/V_0=0.9$ . For GdRu<sub>2</sub>Si<sub>2</sub> the

TABLE II. Mössbauer results of high-pressure measurements on three intermetallic compounds at 4.2 K.

Compound	$p$ GPa	$V/V_0$	$V_{zz}$ $10^{21} \text{ V m}^{-2}$	$B_{\text{hf}}$ T	IS mm/s	$\theta$ deg
GdCo <sub>5</sub>	0	1.000	+10.1	-7.45	0.24	0
	3.0	0.960	+9.9	-1.1	0.20	0
	5.4	0.937	+10.1	-1.9	0.19	0
	9.6	0.875	+9.8	0	0.16	0
	14.0	0.841	+9.4	(-)1.1	0.12	0
	18.0	0.805	+8.9	(-)6.2	0.10	0
GdRu <sub>2</sub> Si <sub>2</sub>	0	1.00	-18.45	-28.2	0.43	50
	4.1	0.96	-18.5	-26.4	0.39	50
	6.0	0.95	-18.8	-26.2	0.37	50
	9.1	0.92	-19.2	-26.4	0.35	50
	17.9	0.83	-19.1	-25.5	0.30	50
Gd <sub>2</sub> Co <sub>17</sub> N <sub>3</sub>	0	1.000	+14.9	-10.3	0.45	0
	4.2	0.965	+16.2	-4.8	0.42	0
	9.8	0.919	+16.0	(-)7.9	0.38	0

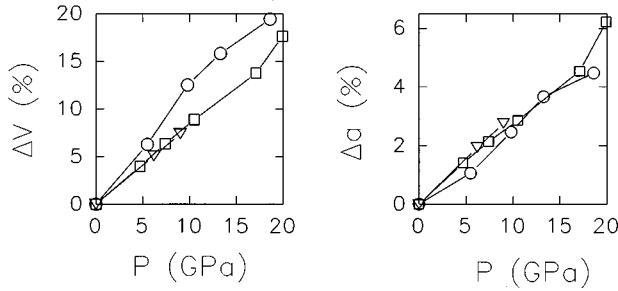


FIG. 3. Pressure-volume relations, and the pressure dependences of the length of the  $a$  axis, of the compounds  $\text{GdCo}_5$  (circles),  $\text{GdRu}_2\text{Si}_2$  (squares), and  $\text{Gd}_2\text{Co}_{17}\text{N}_3$  (triangles).

$c/a$  ratio varies less than 1% across the pressure interval studied. Calculations of the effect of  $c/a$  changes have therefore not been performed.

## V. DISCUSSION

### A. Magnetic moments and hyperfine fields

First we discuss the volume dependence of the site-resolved magnetic moments, as obtained from the band-structure calculations. Whereas the  $4f$  contribution to the moment is stable, the valence electron contribution decreases in all systems with pressure. The data given in Table III show that the dominant contribution to the moments, and to their pressure dependence, results from the  $5d$  electrons. The decrease of the induced  $5d$  moment with pressure results from two effects. First, the application of pressure widens the  $5d$  band, which therefore becomes less polarizable. This is

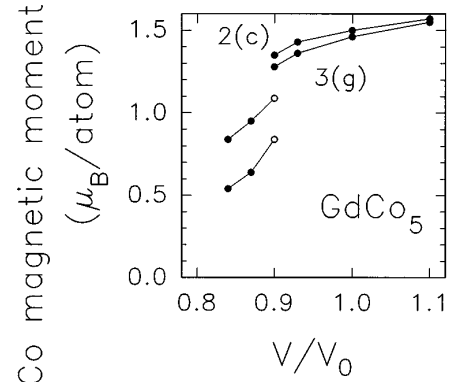


FIG. 4. The calculated magnetic moments of the Co atoms at the  $2c$  and  $2g$  sites of  $\text{GdCo}_5$  plotted vs the normalized volume.

the dominant effect for elemental Gd and for  $\text{GdRu}_2\text{Si}_2$ . In these systems the  $5d$  polarization originates exclusively from the interaction with the Gd- $4f$  moments, which remain constant. A second and much larger effect is observed for  $\text{GdCo}_5$ , in which the  $5d$  shell is polarized by the on-site  $4f$  shell, as well as by the direct exchange interaction with the spin split Co- $3d$  states.  $\text{GdCo}_5$  is a strong ferromagnet, with the majority spin  $3d$  shell fully occupied at  $p=0$ . Therefore, the pressure dependence of the Co moment is relatively weak around  $p=0$ . However, upon the application of pressure the  $3d$  bands broaden, and a transition occurs to weak ferromagnetism, with a high density of majority and minority Co- $3d$  states at the Fermi level. As a result, the pressure dependence of the Co moments is much larger, and the moments decrease rapidly. As shown in Fig. 4, this decrease is even

TABLE III. Calculated volume dependence of partial and total moments at Gd sites in Gd(hcp), Gd(fcc), Gd(dhcp) [cubic ( $c$ ) and hexagonal ( $h$ ) sites],  $\text{GdCo}_5$ , and  $\text{GdRu}_2\text{Si}_2$ . The total moment includes the  $4f$  contribution. The calculated  $4f$  moment is slightly lower than  $7\mu_B$ , as the result of a small occupation of  $4f$  minority spin states. In all cases, the difference is less than  $0.1\mu_B$ . Units:  $\mu_B$  per atom. The error in  $\mu_{\text{tot}}$  is  $\pm 0.01\mu_B$ .

System	$\frac{V}{V_0}$	$\mu_s$	$\mu_p$	$\mu_d$	$\mu_{\text{tot}}$
Gd(hcp)	1.00	0.019	0.161	0.562	7.74
	0.97	0.020	0.156	0.554	7.73
	0.94	0.021	0.154	0.556	7.73
	0.91	0.023	0.151	0.552	7.72
	0.88	0.025	0.147	0.548	7.71
Gd(fcc)	1.00	0.012	0.163	0.558	7.73
Gd(dhcp)	1.00	0.008	0.152	0.489	7.66 (c)
		0.019	0.141	0.497	7.65 (h)
	0.80	0.011	0.105	0.365	7.47 (c)
		0.023	0.094	0.370	7.46 (h)
$\text{GdCo}_5$	1.10	0.041	0.105	0.459	7.54
	1.00	0.041	0.089	0.419	7.50
	0.90	0.041	0.073	0.391	7.43
	0.84	0.031	0.037	0.266	7.26
$\text{GdRu}_2\text{Si}_2$	1.00	0.017	0.023	0.176	7.16
	0.91	0.016	0.022	0.168	7.13
	0.83	0.015	0.020	0.160	7.10

TABLE IV. Calculated dependence on the  $c/a$  ratio of the magnetic moments, electric-field gradients, and hyperfine fields for hcp Gd and GdCo<sub>5</sub>. Note that the ideal hcp structure is obtained for  $c/a=(8/3)^{1/2}=1.633$ , and that the experimental value for hcp-Gd is equal to  $c/a=1.59047$ .

System	$V/V_0$	$c/a$	$\mu_{\text{tot}}$ ( $\mu_B$ )	$V_{zz}(\text{val})$ ( $10^{21} \text{ V m}^{-2}$ )	$B_{\text{hf}}^{\text{calc}}$ (T)
Gd(hcp)	1.0	1.68	7.73	-1.9	-7.5
		1.633	7.73	+1.6	-7.0
		1.59047	7.73	+3.8	-6.0
		1.56	7.72	+6.6	-4.3
		1.53	7.72	+8.0	-2.4
GdCo <sub>5</sub>	0.9	0.79811	7.43	+13.7	+40.5
		0.764	7.43	+14.2	+38.7

expected to be discontinuous at a reduced volume of about 0.90. At the same time, the induced Gd-5*d* polarization decreases rapidly with pressure.

Whereas the 6*p* and 5*d* partial (orbital resolved) magnetic moments more strongly contribute to the magnetization, the hyperfine field is most sensitive to the 6*s* partial magnetic moment. An expression for the relation between the partial magnetic moments and the hyperfine field has been given by Eq. (A1) in the previous section. Although it has been derived from calculational results for systems at zero pressure, it is shown in Fig. 5 that it also provides a fair description of the pressure dependence of the calculated hyperfine fields, in terms of the pressure dependence of the partial magnetic moments. The figure gives estimated values of the hyperfine field, using Eq. (A1), for all systems and volumes for which calculated moments are given in Table III, as a function of the actually calculated hyperfine fields [ $B_{\text{hf}}(\text{calc}) = -12 \text{ T}$  for fcc-Gd at  $V=V_0$ , other data taken from Tables III–VI]. Table III shows that the 6*s* partial magnetic moment, and hence the hyperfine field, is very sensitive to structural details: for fcc Gd, the 6*s* magnetic moment is only about half the value obtained for hcp Gd, and a similar difference is

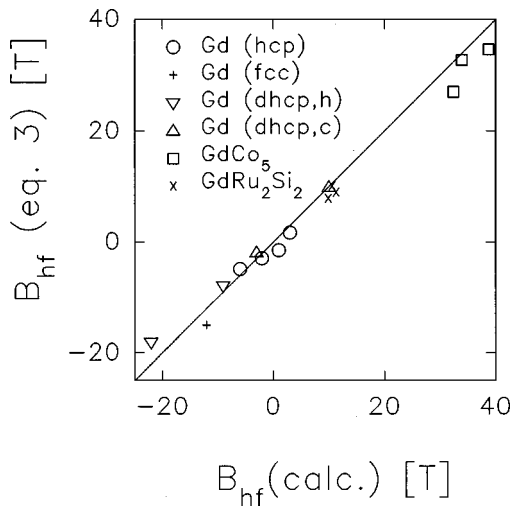


FIG. 5. Comparison of hyperfine fields estimated from partial (orbital resolved) magnetic moments [using Eq. (A1)], with actually calculated hyperfine fields. The figure includes results for all systems and volumes for which data are given in Table II.

obtained for the cubic and hexagonal sites in dhcp Gd. We note that, experimentally, the two hyperfine subspectra have not been resolved (Table I).

Upon making a comparison between calculated and experimental hyperfine fields, we will concentrate on *changes* with volume, rather than the absolute values, in view of the systematic error in calculated hyperfine fields at zero pressure (see Sec. IV). For hcp and dhcp Gd, and for GdCo<sub>5</sub> at moderate pressures, the calculations predict stable or slightly increasing 6*s* partial magnetic moments with pressure, and a decrease of the sum of the 6*p* and 5*d* partial moments (see Table III). In such a case, the application of Eq. (A1) predicts that the hyperfine field becomes larger (more positive) with pressure. The predicted trend is in agreement with the experimental observations. However, the experimental increase is much larger than predicted. For hcp Gd, from  $V=V_0$  to  $V=0.94V_0$ , the difference is about a factor 2, and for GdCo<sub>5</sub>, from  $V=V_0$  to  $V=0.9V_0$ , the difference is a factor 3–4. Whereas the calculated hyperfine fields of hcp Gd (at  $V=V_0$ ) and dhcp Gd (at  $V=0.8V_0$ , average of the cubic and hexagonal sites) differ by only +6.5 T, the experimentally observed increase of the hyperfine field is +29 T. For GdCo<sub>5</sub>, the calculations predict that the hyperfine field shows a maximum, and decreases upon decreasing the unit cell volume below a reduced volume of  $V/V_0=0.9$ . Unfortunately, the sign of the hyperfine field could not be determined experimentally, and the experimental maximum of the hyperfine field (if there is a maximum) has a value close to zero, so we cannot tell whether the prediction is (at least qualitatively) correct.

For GdRu<sub>2</sub>Si<sub>2</sub> the 6*s*, 6*p*, and 5*d* polarizations all decrease with pressure, leading to opposing contributions to the pressure dependence of the hyperfine field. Experimentally,  $B_{\text{hf}}$  increases slightly with pressure, but with a rate which is much smaller than for Gd and GdCo<sub>5</sub>.

In conclusion, calculated hyperfine fields (and their pressure dependence) are strongly correlated to calculated partial magnetic moments (and their pressure dependence). However, the predicted pressure dependence of hyperfine fields agrees at best only qualitatively with the experimental results. For Gd and GdCo<sub>5</sub> the change of the hyperfine field with pressure, close to  $V=V_0$ , is underestimated by a factor 2–4 by the calculations.

TABLE V. Results of calculations for hcp Gd at different pressures  $P$  (in GPa).  $\Delta n$  is defined as in Eq. (2),  $\langle r^{-3} \rangle$  is expressed in  $a_0^{-3}$ ,  $V_{zz}(\text{val})$  is the sum of the four contributions of the different orbitals and spin states.  $V_{zz}$  is expressed in  $10^{21} \text{ V m}^{-2}$ , the calculated Gd moment  $\mu^{\text{calc}}$  in  $\mu_B$ , and the hyperfine fields  $B_{\text{hf}}$  in T.

$V/V_0$	$P$		$\Delta n$	$\left\langle \frac{S(r)}{r^3} \right\rangle$	$V_{zz}(\text{val})$	$V_{zz}^{\text{expt}}$	$B_{\text{hf}}^{\text{calc}}$	$B_{\text{hf}}^{\text{expt}}$
1.00	0	$6p \uparrow$	0.0199	19.7	3.8	3.8	-6	-40
		$6p \downarrow$	0.0021	21.3				
		$5d \uparrow$	0.0267	2.18				
		$5d \downarrow$	0.0008	1.72				
0.97	0.7	$6p \uparrow$	0.0208	21.9	4.2		-2	
		$6p \downarrow$	0.0018	23.7				
		$5d \uparrow$	0.0253	2.22				
		$5d \downarrow$	0.0017	1.77				
0.94	1.6	$6p \uparrow$	0.0213	23.1	4.6	4.8	+1	-28
		$6p \downarrow$	0.0021	25.1				
		$5d \uparrow$	0.0240	2.24				
		$5d \downarrow$	0.0026	1.80				
0.90	3.0	$6p \uparrow$	0.0208	24.9	4.8		+3	
		$6p \downarrow$	0.0022	27.1				
		$5d \uparrow$	0.0234	2.28				
		$5d \downarrow$	0.0032	1.83				

### B. Electric-field gradients

For the systems studied, the observed relative changes with pressure of the EFG's are much smaller than the relative changes of the hyperfine field. The largest relative change was observed for Gd: an increase of the EFG at the hexagonal sites of about a factor 2, from  $+3.8 \times 10^{21} \text{ V m}^{-2}$  for  $V/V_0=1$  to  $+8 \times 10^{21} \text{ V m}^{-2}$  for  $V/V_0=0.7$  (Table I). For hcp Gd theory and experiment compare favorably:  $V_{zz}$  is about 25% larger for  $V/V_0=0.94$  than for  $V/V_0=1.0$ . As shown by Table V, the increase of the EFG with pressure is the combined effect of an increasing value of  $\langle S(r)/r^3 \rangle$  and  $\Delta n$  [mainly ( $6p \uparrow$ ) values]. However, whereas experiment shows that this trend for the EFG on the hexagonal sites is continued after the transition to the Sm-type phase and finally the dhcp phase, assuming  $V_{zz}=0$  on the cubic sites, theory predicts (i) that the EFG at the hexagonal site in dhcp Gd at  $V/V_0=0.8$  is significantly smaller than the value derived from experiment ( $4.2$  versus  $6.4 \times 10^{21} \text{ V m}^{-2}$ ), and (ii) that the EFG at the cubic site is not equal to zero, and in fact not much smaller than the EFG at the hexagonal sites. We note that the ‘‘cubic’’ sites only have a cubic nearest neighbor environment, and that the actual crystallographic

point symmetry is lower, allowing a nonzero EFG due to interactions with atoms outside the first shell of nearest neighbor atoms. Apparently, these interactions are non-negligible in the case of dhcp Gd.

For  $\text{GdCo}_5$  and  $\text{GdRu}_2\text{Si}_2$  the experimental volume dependences of the EFG's are quite small. In the case of  $\text{GdCo}_5$  the calculated changes in the EFG are larger than the experimental changes, and they have the opposite sign. The large calculated increase of  $V_{zz}$  with pressure is related to a strong increase of calculated  $\langle S(r)/r^3 \rangle$  values (see Table VII). For  $\text{GdRu}_2\text{Si}_2$  the calculated and experimental values of  $V_{zz}$ , for  $V/V_0=1.0$  and  $V/V_0=0.83$ , agree within a few percent. Although, in view of the error margins involved, this agreement is satisfactory, a significant disagreement (about 20%) is observed for  $V/V_0=0.91$  (see Table VIII). As shown by the table, the predicted ‘‘dip’’ in the EFG at  $V/V_0=0.91$  is related to a relatively low value of  $\langle S(r)/r^3 \rangle_{6p}$ . An analysis of the origin of errors in the predicted volume dependence of  $V_{zz}$  is beyond the scope of this paper. It should be based on a comparison with results from full potential band structure calculations, such as presented in<sup>21</sup> for  $\text{Gd}_2\text{Fe}_{17}\text{X}_3$  ( $X=\text{C}$  and  $\text{N}$ ) and  $\text{GdCo}_5$  at zero pressure, and it should include possible contributions due to semicore ( $5p$ ) orbitals.

TABLE VI. The results at different pressures  $P$  (in GPa) for the calculated and experimental EFG's ( $V_{zz}^{\text{cub,hex,expt}}$  in  $10^{21} \text{ V m}^{-2}$ ), the calculated moments ( $\mu_{\text{cub,hex}}$  in  $\mu_B$ ), and the calculated and experimental hyperfine fields ( $B_{\text{hf}}^{\text{cub,hex,expt}}$  in T) at the Gd nuclei in the high-pressure dhcp phase of Gd.

$V/V_0$	$P$	$V_{zz}^{\text{cub}}$	$V_{zz}^{\text{hex}}$	$V_{zz}^{\text{expt}}$	$\mu^{\text{cub}}$	$\mu^{\text{hex}}$	$B_{\text{hf}}^{\text{cub}}$	$B_{\text{hf}}^{\text{hex}}$	$B_{\text{hf}}^{\text{expt}}$
1.00	0	2.3	4.0		7.65	7.66	-22	-3	
0.80	8.2	3.3	4.2	6.4	7.46	7.47	-9	10	-11

TABLE VII. Band-structure calculation results for GdCo<sub>5</sub>. The pressure is given in GPa,  $\Delta n$  is defined as in Eq. (2),  $\langle r^{-3} \rangle$  in  $a_0^{-3}$ ,  $V_{zz}$  in  $10^{21}$  V m<sup>-2</sup>, and  $B_{\text{hf}}$  in T.  $\mu^{\text{calc}}$  represents, respectively, the calculated moments of Gd, Co (2c site), and Co (3g site) (given in vertical order for each value of the pressure).

$\frac{V}{V_0}$	$P$		$\Delta n$	$\left\langle \frac{S(r)}{r^3} \right\rangle$	$V_{zz}(\text{val})$	$V_{zz}^{\text{expt}}$	$\mu^{\text{calc}}$	$B_{\text{hf}}^{\text{calc}}$	$B_{\text{hf}}^{\text{expt}}$
1.10	-8	6p↑	0.0272	25.2	10.9		7.54	+33.9	
		6p↓	0.0259	22.4			-1.57		
		5d↑	0.0558	1.30			-1.55		
		5d↓	0.0704	1.85					
1.00	0	6p↑	0.0267	30.5	12.3	10.1	7.50	+38.7	-7.5
		6p↓	0.0234	26.9			-1.50		
		5d↑	0.0598	1.38			-1.46		
		5d↓	0.0583	1.90					
0.90	9	6p↑	0.0260	37.5	14.1	10.0	7.43	+41.2	(-)1
		6p↓	0.0221	32.9			-1.35		
		5d↑	0.0590	1.50			-1.28		
		5d↓	0.0461	1.98					
0.84	15	6p↑	0.0246	42.4	14.5	9.5	7.26	+32.4	(-)1.5
		6p↓	0.0180	37.8			-0.84		
		5d↑	0.0630	1.59			-0.54		
		5d↓	0.0536	1.99					

## VI. CONCLUSIONS

In this paper experimental results on the pressure dependence of the <sup>155</sup>Gd hyperfine parameters of Gd, GdCo<sub>5</sub>, GdRu<sub>2</sub>Si<sub>2</sub>, and Gd<sub>2</sub>Co<sub>17</sub>N<sub>3</sub> have been presented. Using pressures up to 18 GPa, significant changes of the EFG, hyperfine fields, and isomer shifts have been observed. In order to be able to interpret the observations in terms of the pressure dependence of magnetic moments and the electron density distribution, first-principles ASW band-structure calculations of the EFG and hyperfine fields have been performed. As a first result, we have formulated a quantitative relationship

[Eq. (A1)] between the calculated hyperfine field at Gd sites and the calculated partial magnetic moments at Gd sites. It is quite accurate for a large number of compounds at zero pressure, as well as at elevated pressures for the systems studied in this paper, and reveals how the hyperfine fields are related to the 6s moments and (indirectly) to the much larger 6p and 5d moments.

In spite of earlier findings that first principles predictions of the EFG and hyperfine fields at Gd nuclei in compounds at zero pressure are quite accurate, we have found that first principles calculations of the pressure dependence for elemental Gd, GdCo<sub>5</sub>, and GdRu<sub>2</sub>Si<sub>2</sub> do not in all cases lead to

TABLE VIII. Band-structure calculation results for GdRu<sub>2</sub>Si<sub>2</sub>. The pressure is given in GPa,  $\Delta n$  is defined as in Eq. (2) ( $r^{-3}$ ) in  $a_0^{-3}$ ,  $V_{zz}(\text{val})$  in  $10^{21}$  V m<sup>-2</sup>, and the hyperfine fields  $B_{\text{hf}}$  in T. The calculated moments  $\mu^{\text{calc}}$  represent the Gd, Ru, and Si moments, respectively (top to bottom).

$P$	$\frac{V}{V_0}$		$\Delta n$	$\left\langle \frac{S(r)}{r^3} \right\rangle$	$V_{zz}(\text{val})$	$V_{zz}^{\text{expt}}$	$\mu^{\text{calc}}$	$B_{\text{hf}}^{\text{calc}}$	$B_{\text{hf}}^{\text{expt}}$
0	1.00	6p↑	-0.0317	35.0	-17.9	-18.5	7.20	+10.6	-28.2
		6p↓	-0.0296	39.5			-0.05		
		5d↑	-0.0244	2.00			0		
		5d↓	-0.0325	1.64					
11	0.91	6p↑	-0.0304	30.3	-15.8	-19.2	7.13	+11.3	-26.4
		6p↓	-0.0283	33.8			-0.04		
		5d↑	-0.0230	1.99			0		
		5d↓	-0.0211	1.61					
20	0.83	6p↑	-0.0294	41.4	-19.2	-19.1	7.10	+9.9	-25.5
		6p↓	-0.0264	46.1			-0.03		
		5d↑	-0.0183	2.15			0		
		5d↓	-0.0149	1.81					

a satisfactory agreement with experiment. The calculated pressure dependence of hyperfine fields is too small by a factor 2-5. The calculated pressure dependence of  $V_{zz}$  agrees satisfactorily with experiment for hcp Gd (small pressures), but shows, in the case of  $\text{GdCo}_5$ , even the wrong sign. We expect that these results will stimulate the formulation of improved theory and calculational methods for hyperfine parameters, and conclude that experimental studies of the pressure dependence of hyperfine parameters provide a critical test for such new developments.

#### ACKNOWLEDGMENTS

We acknowledge the use of the x-ray DAC of the Free University in Amsterdam and the image plates of the Onze Lieve Vrouwe Gasthuis in Amsterdam. The experimental advice of R. J. Wijngaarden and D. de Groot is gratefully acknowledged. This work was part of the research program of the ‘‘Stichting voor Fundamenteel Onderzoek der Materie’’ (FOM), which was financially supported by the ‘‘Nederlandse Organisatie voor Wetenschappelijk Onderzoek’’ (NWO).

#### APPENDIX

More insight into the various contributions to hyperfine fields at Gd may be obtained by analyzing the relationship with the partial magnetic moments  $\mu_s$ ,  $\mu_p$ , and  $\mu_d$  at Gd sites due to  $6s$ ,  $6p$ , and  $5d$  valence electrons, respectively. The partial moments may be obtained from the ASW band-structure calculations by integrating the wave-function-resolved spin densities over the Gd Wigner-Seitz spheres. A first contribution to the hyperfine field is due to the polarization of  $s$ -type core states by the spin-polarized  $4f$  states. The spin-polarization of  $6s$  valence states, with a finite electron density near the nucleus, leads to an additional direct contribution to the hyperfine field. On the other hand, the polarization of  $6p$  and  $5d$  states only has an indirect effect on the hyperfine field, by modifying the spin polarization near the nucleus due to the  $s$ -type core states.

For all systems studied in Ref. 17,  $\mu_s$  is one order of magnitude smaller than  $\mu_d$ , whereas  $\mu_p$  varies typically between 0.1 and 0.3 times  $\mu_d$ .<sup>22</sup> From a study of the  $s$ ,  $p$ , and  $d$  contributions to the hyperfine field by analyzing the data presented in Ref. 17 we conclude that, in spite of the small value of  $\mu_s$ , the direct  $6s$  contribution is quite important. This may be seen by inspection of Fig. 1 in Ref. 17, which displays for a large number of intermetallic compounds the calculated hyperfine field  $B_{\text{hf}}^{\text{calc}}$  as a function of  $\mu_s$ . These quantities are strongly correlated. The largest deviation from a best fit is obtained for systems such as Gd and  $\text{GdZn}$ , which have an exceptionally high ratio  $(\mu_p + \mu_d)/\mu_s$ , viz.,

about 30. For these systems, the hyperfine field is about 20 T lower than expected from a best fit of  $B_{\text{hf}}^{\text{calc}}$  versus  $\mu_s$ . One may take this negative contribution from non- $s$  electrons into account by fitting the calculated data using the relationship

$$B_{\text{hf}}^{\text{calc}} = B_{\text{hf}}^0 + a_s \mu_s + a_{p,d} (\mu_p + \mu_d). \quad (\text{A1})$$

Our set of calculated data was not varied enough to distinguish  $p$  and  $d$  contributions. In order to keep the parametrization as simple as possible,  $p$  and  $d$  moments are summed, and a single  $a_{p,d}$  parameter is used. We have found that expression (A1) describes the calculated variation of hyperfine fields within a few T, using  $B_{\text{hf}}^0 = -8 \pm 3$  T,  $a_s = 1460 \pm 50$  T/ $\mu_B$ , and  $a_{p,d} = -34 \pm 7$  T/ $\mu_B$ .<sup>23</sup>

We would like to make two comments concerning the parametrization of hyperfine fields in terms of partial moments. First, we emphasize that the definition of partial magnetic moments is specific to the band-structure method used (in particular, to the choice of the basis set and to the size of Wigner-Seitz sphere radii). Hence, the parameter values obtained from the fit are at best only valid in this specific context. Second, the coefficients  $a_l$  ( $l = s, p, d$ ) are determined by the specific shape of the Gd  $6s$ ,  $6p$ , and  $5d$  wave functions, which depends on the environment of the Gd atoms studied. The set of parameters given above has been derived from data on metallic systems at zero pressure. It cannot be excluded that the  $a_l$  coefficients change appreciably with the degree of ionicity of the bonds between Gd and its environment, or with pressure. However, we regard parametrization useful as a means of obtaining more physical insight. The validity of this parametrization scheme to hyperfine fields for systems under pressure was discussed in Sec. V.

It is of interest to remark that there is strong experimental evidence for opposite contributions of  $s$ - and  $d$ -type valence electron polarization to the Gd hyperfine field. From the analysis of hyperfine fields and magnetic ordering behavior of Gd-based compounds containing nonmagnetic  $^{139}\text{La}$  probe atoms, Dorman<sup>24</sup> has concluded that  $a_d/a_s \sim -0.1$ . In addition, we remark that the term  $B_{\text{hf}}^0$  in Eq. (1) may be associated with the contribution  $B_{\text{hf}}^C$  due to the polarization of core  $s$  electrons due to the  $4f$  moment on the same atom. Experimental work on highly ionic systems, for which no other contribution is expected, should reveal this term directly. One often assumes that  $B_{\text{hf}}^0 \sim -33.2$  T, as obtained from the hyperfine field at Gd in gadolinium iron garnet<sup>25</sup> and other systems with Gd in a highly oxidized state. This value may be compared to the value of  $B_{\text{hf}}^0$ , given above, which after the above-mentioned correction for the systematic error in the calculations of about 35 T becomes  $-43$  T.

<sup>1</sup>K. H. J. Buschow, Rep. Prog. Phys. **54**, 1123 (1991).

<sup>2</sup>R. Coehoorn, K. H. J. Buschow, M. W. Dirken, and R. C. Thiel, Phys. Rev. B **42**, 4645 (1990).

<sup>3</sup>R. Coehoorn, in *Supermagnets, Hard Magnetic Materials*, Lec-

ture Notes NATO-ASI, edited by G. J. Long and F. Grandjean (Kluwer, Dordrecht, 1990).

<sup>4</sup>K. H. J. Buschow, R. Coehoorn, F. M. Mulder, and R. C. Thiel, J. Magn. Magn. Mater. **118**, 347 (1993).

- <sup>5</sup>F. M. Mulder, J. H. V. J. Brabers, R. C. Thiel, K. H. J. Buschow, and F. R. de Boer, *J. Alloys Compd.* **1**, 118 (1995).
- <sup>6</sup>F. M. Mulder and R. C. Thiel, *Europhys. Lett.* **25**, 657 (1994).
- <sup>7</sup>R. D. Taylor and M. P. Pasternak, *Hyperfine Interact.* **53**, 159 (1990).
- <sup>8</sup>F. M. Mulder and R. C. Thiel, *Rev. Sci. Instrum.* **65**, 707 (1994).
- <sup>9</sup>R. A. Forman, G. J. Piermarini, J. D. Barnett, and S. Block, *Science* **176**, 284 (1972).
- <sup>10</sup>J. D. Barnett, S. Block, and G. J. Piermarini, *Rev. Sci. Instrum.* **44**, 1 (1973).
- <sup>11</sup>J. Akella, G. S. Smith, and A. P. Jephcoat, *J. Phys. Chem. Solids* **49**, 573 (1988).
- <sup>12</sup>W. A. Groshans and W. B. Holzapfel, *Phys. Rev. B* **45**, 5171 (1992).
- <sup>13</sup>K. Takemura and K. Syassen, *J. Phys. F* **15**, 543 (1985).
- <sup>14</sup>R. J. Nelmes, P. D. Hatton, M. I. McMahon, R. O. Piltz, and J. Crain (unpublished).
- <sup>15</sup>H. de Graaf, Ph.D. thesis, Leiden, 1982.
- <sup>16</sup>S. Blügel, H. Akai, R. Zeller, and P. H. Dederichs, *Phys. Rev. B* **35**, 3271 (1987).
- <sup>17</sup>R. Coehoorn and K. H. J. Buschow, *J. Magn. Magn. Mater.* **118**, 175 (1993).
- <sup>18</sup>R. Coehoorn, *J. Magn. Magn. Mater.* (to be published).
- <sup>19</sup>H. Ebert, P. Strange, and B. L. Gyorffy, *J. Phys. F* **18**, L135 (1988).
- <sup>20</sup>P. Villars and L. D. Calvert, in *Pearson's Handbook of Crystallographic Data for Intermetallic Phases* (ASM International, Ohio, 1991).
- <sup>21</sup>R. Coehoorn and G. H. O. Daalderop, *J. Magn. Magn. Mater.* **104**, 1081 (1992).
- <sup>22</sup>It should be noted that the upper limit of the horizontal scale in Fig. 2 of Ref. 17 should be 1.0 (instead of 0.1)  $\mu_B$ .
- <sup>23</sup>R. Coehoorn (unpublished).
- <sup>24</sup>E. Dorman, *J. Magn. Magn. Mater.* **6**, 87 (1977).
- <sup>25</sup>Le Dang Khoi, *Phys. Lett.* **28A**, 671 (1969).